Comparing Robust and Physics-Based Sea Surface Temperature Retrievals for High Resolution, Multi-Spectral Thermal Sensors Using one or Multiple Looks

Christoph C. Borel, William B. Clodius, John J. Szymanski and James Theiler
Space and Remote Sensing Sciences Group
NIS-Division, Mailstop C323, Los Alamos National Laboratory
Los Alamos, NM 87545, USA
cborel@lanl.gov

ABSTRACT

With the advent of multi-spectral thermal imagers such as EOS's ASTER high spatial resolution thermal imagery of the Earth's surface will soon be a reality. Previous high resolution sensors such as Landsat 5 had only one spectral channel in the thermal infrared and its utility to determine absolute sea surface temperatures was limited to 6-8 K for water warmer than 25 deg C. This inaccuracy resulted from insufficient knowledge of the atmospheric temperature and water vapor, inaccurate sensor calibration, and cooling effects of thin high cirrus clouds. We will present two studies of algorithms and compare their performance. The first algorithm we call "robust" since it retrieves sea surface temperatures accurately over a fairly wide range of atmospheric conditions using linear combinations of nadir and off-nadir brightness temperatures. The second we call "physics-based" because it relies on physics-based models of the atmosphere. It attempts to come up with a unique sea surface temperature which fits one set of atmospheric parameters.

Keywords: sea surface temperature retrieval, cirrus cloud detection, multi-angular retrieval, multi-spectral thermal sensors

1. Introduction

Modern multi-spectral sensors have both more bands and better calibration. Additional knowledge about the atmosphere can be derived using bands located in atmospherically interesting regions such as the water vapor band near 0.94 μm and the cirrus band near 1.37 μm. Most often however the atmospheric parameters must be retrieved from the data itself. Such an approach is the split-window technique (Sobrino et al, 1993) which is used for 3 channel data from AVHRR.

An example of how different the observed top-of-atmosphere (TOA) brightness temperatures can be for different atmospheres is shown in Fig. 1. For a given measured brightness temperature of 290 K we could have an sea surface temperature (SST) ranging from 294 to 298 K in the mid-wave (MWIR) and 292 to 301 in the long-wave (LWIR). The errors increase with higher SST. Note that the referred atmospheric cases (A, B and C) in Fig. 1 do not correspond to the cases used in section 4. The starting point (case A) is a US standard atmosphere with a columnar water vapor amount of 0.74 g/cm^2, tropospheric aerosol and no cirrus cloud. Case B is obtained by replacing the aerosol by urban aerosol with 5 km visibility. Case C adds a high visible cirrus cloud and case D increases the columnar water vapor amount of 3.5 g/cm^2.

Two approaches were investigated. The first we call "robust" because it retrieves sea surface temperatures quite accurately over a fairly wide range of atmospheric conditions using linear combinations of nadir and off-nadir brightness temperatures as observed in multiple spectral bands. An advantage of the robust method is that it requires no additional input about the atmosphere, e.g. meteorological information. We quantify how two looks improve the sea surface temperature accuracy. The second algorithm we call "physics-based" because it uses measured atmospheric parameters in radiative transfer computations to derive water vapor, effective atmospheric temperature and sea surface temperature simultaneously. The advantage of the "physical" method is that we can incorporate additional information, e.g. from other spectral channels and meteorological data.

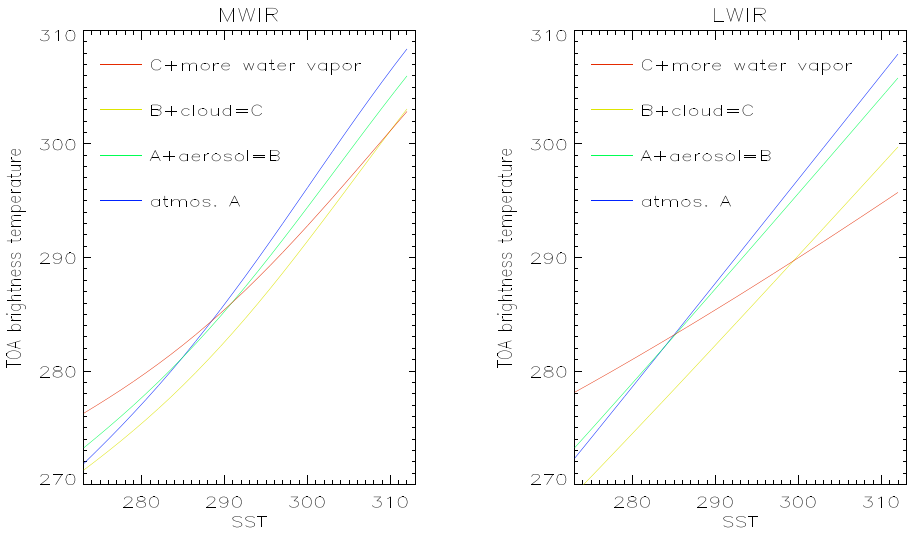

Figure 1. Sea surface temperature and spectral top-of-atmosphere (TOA) brightness temperature for different atmospheres for the mid-wave and long-wave infrared. See text for details on atmospheric cases.

2. Simulation of a multi-spectral thermal image for a diffraction limited instrument

In order to test the retrievals, we constructed test data using artificial and measured temperature distributions. We also studied the effects of the system point spread function, system noise and calibration accuracy on the temperature retrieval accuracy. Assuming a diffraction limited telescope the blur spot diameter (related to the width of the point spread function) in the mid-wave channels is about half the size in the long-wave infrared. Thus a land-water boundary would appear sharper in the MWIR than in the LWIR for the same ground sampling distance (GSD). Various image restoration methods were investigated to sharpen the LWIR imagery near land/water boundaries and to recover details lost by the increased GSD of off-nadir looks. Another approach to retrieve sub-pixel temperatures is described in another paper in this conference by J. Szymanski et al, 1999. The flow of data from the ground up to the sensor and into the data processing chain for the simulation of multi-spectral imagery in the thermal is shown in Fig. 2 for the nadir view data. A similar data stream exists for the off-nadir views with 2,...,5 channels depending on the set of weighting coefficients.

Each module will now be described in some detail.

2.1. Temperature map:

The temperature map $T_w(x, y)$ was derived for two types of scenes:

1. Artificial non-uniform checkerboard patterns of different widths and with two temperatures (see Fig. 3.a).
2. A temperature map derived from multi-fractal simulation of ponds in a variable land temperature background (see Fig. 3.b).

2.2. Atmospheric effects simulation:

An atmospheric radiative transfer code (MODTRAN 2) was used to simulate the atmosphere. Three different standard atmospheres were used to describe most atmospheric conditions: polar, US-standard and tropical atmospheres. Since each atmospheres has a unique water vapor profile we scaled the amount of water vapor for tropical between 1.5 and 4.2 g cm^{-2} in eleven steps, for US-standard between 0.74 and 2.1 g cm^{-2} in five steps and for polar between 0.09 and 0.37 g cm^{-2} in four steps. Thus we generated 20 different atmospheric states. For each of them we considered urban (visibility is 5 km), rural (visibility is 23 km) and tropospheric

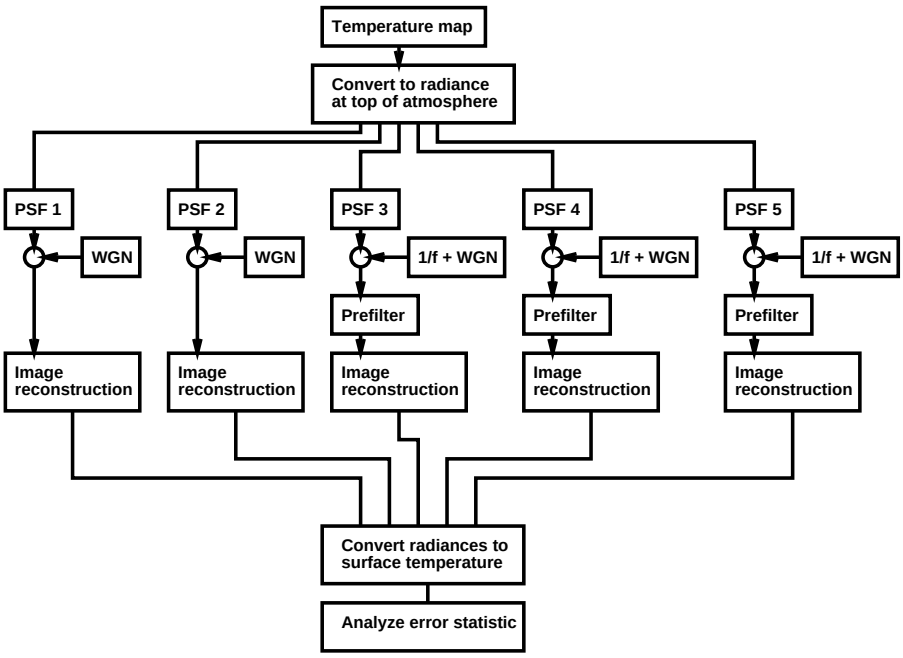

Figure 2. Flow diagram to compute the temperature error for a simulated 5 channel multi-spectral thermal scene see Table 2 for band limits. Abbreviations: "1/f" stands for correlated noise, WGN stands for "white Gaussian noise" and PSF for the system "point spread function".

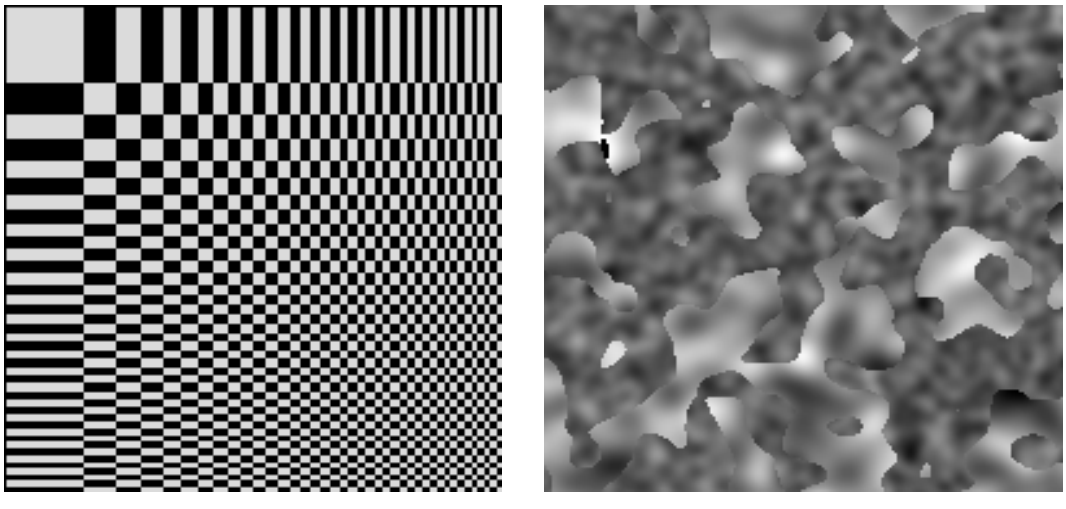

Figure 3. Temperature maps $T_w(x,y)$ used: a. non-uniform checkerboard pattern and b. multi-fractal ponds

Channel : 1					Channel : 2				
0	1	2	1	0	1	1	2	1	1
1	10	40	10	1	1	13	49	13	1
2	108	615	108	2	3	108	578	108	3
1	13	51	13	1	1	15	58	15	1
0	1	2	1	0	1	1	2	1	1

Channel : 3					Channel : 4					Channel : 5				
0	1	2	1	0	1	2	3	2	1	1	2	3	2	1
2	18	65	18	2	2	18	63	18	2	2	24	77	24	2
3	110	472	110	3	3	108	474	108	3	4	112	405	112	4
2	24	83	24	2	2	23	81	23	2	3	29	91	29	3
1	2	3	2	1	1	2	3	2	1	1	3	4	3	1

Table 1. Table of normalized point spread functions used in simulation. The motion is from left to right.

(visibility is 50 km) aerosols. To apply the temperature retrieval to non-ideal situations we included cloud free conditions with and without volcanic aerosols as well as the possible existence of a cirrus cloud. The cirrus was varied in its geometrical thickness (0.2km, 0.5km and 0.9km) and heights (6km and 10km). Thus, we produced $N = (20 \cdot 3) \cdot (2 + 2 \cdot 3) = 480$ types of different model atmospheres. Using the MODTRAN output files for all $j = 1, ..., 480$ cases the over band i averaged top-of-atmosphere (TOA) radiance images $L_{i,j}(x,y)$ can be calculated as a function of SST $T_w(x,y)$:

$$L_{i,j}(T_w(x,y)) \;=\; \sum_{n=0}^{n=4} p_{i,j,n}\,[T_{w,i}(x,y)]^n, \tag{1}$$

where $p_{i,j,n}$ is a polynomial fitting coefficient for the j-th atmospheric state. The error of this fit is less than 0.05% for the LWIR and less than 0.3% for the MWIR. Details of this complex fitting procedure can be found in Tornow et al, 1994.

2.3. Point spread function:

Spatially oversampled point spread functions were computed using the following procedure:

1. For a nominal telescope design we computed wavelength averaged telescope point spread functions (PSF) for each channel i using an optical raytracing code at different locations in the focal plane.
2. Each channel's telescope PSF was then convolved with a linear path (in some cases with additional high-frequency jitter) to simulate the finite integration time of the pixel.
3. Finally the resulting motion and telescope PSF was then integrated over an assumed sensor pixel PSF of a truncated pyramid shape to yield integrated pixel responses for a 5 by 5 pixel array.

In Table 1 we list the computed PSF's, which are normalized to 1000, for all 5 channels whose band limits are listed in Table 2.

2.4. Noise model:

The noise model used consisted of white Gaussian noise (WGN) for the channels 1 and 2 which were assumed to have no drifts and WGN with simulated correlated or $1/f$ noise which was later reduced using a pre-filtering method described in Borel et al, 1996. The pre-filter in the Fourier domain consists of the product of two filters. One filter whitens the correlated noise spectrum, the other is a low-pass filter function e.g. Gaussian or Hanning

window with variable width to block high frequency noise away from the origin of the Fourier Transform of the image data. We optimized the filter parameters for various scenes and found improvements of the root-mean square error (RMSE) of the original minus the pre-filtered noisy image. Additionally, we can study the effect of different signal-to-noise-ratios (SNR) and calibration errors in slope and offset for each pixel.

2.5. Image reconstruction:

Before the sensor measured radiances are converted into a surface temperature we attempt to sharpen the image in such a way that the radiometric accuracy does not suffer and the noise does not increase beyond a certain limit. A number of image reconstruction methods were implemented: Maximum Entropy, Maximum Likelihood, Maximum Residual Likelihood, Goodness of Fit, Weighted Goodness of Fit, Pixon and Iterative Wiener Filtering.

2.6. Converting radiances to surface temperatures:

1. Because we have a finite band width we cannot use the inverse Planck blackbody function. Instead we use a polynomial fit to convert the restored band-integrated radiance $\hat{L}_{w,i}(x,y)$ for the band i image to a brightness temperature map $\hat{T}_{w,i}(x,y)$:

$$\hat{T}_{w,i}(x,y) = \quad = \sum_{n=0}^{5} q_{i,n} \, [\hat{L}_{w,i}(x,y)]^n \tag{2}$$

   where $q_{i,n}$ is a polynomial fitting coefficient.

2. Compute the estimated sea surface temperature $\hat{T}_w(x,y)$ with the robust linear fitting procedure or with a physics-based retrieval method.

3. Compute the root mean square error (RMSE) between the estimated SST's and the true SST over one of $N = 480$ atmospheric cases j for an image of N_x by N_y pixels:

$$RMSE(\hat{T}_w(x,y), T_w(x,y)) = \sqrt{\frac{1}{N_x N_y} \sum_{x=1}^{N_x} \sum_{y=1}^{N_y} (\hat{T}_{w,j}(x,y) - T_w(x,y))^2}$$

2.7. Results:

A simulation program using all previously described modules was written and run for the non-uniform checker pattern in Figure 3.a with two temperatures, 290 and 300 K. The atmosphere selected was a cirrus-free US standard atmosphere with tropospheric aerosols and a water vapor amount of 1.6 g/cm^2. The SNR for WGN was set to 150, 100, 500, 500 and 500 for the five channels (2 in the MWIR and 3 in the LWIR) and the SNR for 1/f noise was set to 1000 for all channels. The resulting histogram of the temperature error shows a smaller standard deviation than if no image restoration was performed. This indicates that boundary pixels moved closer to the SST correct temperature. The systematic temperature error remained about the same for restored vs un-restored SST retrievals.

3. Robust SST retrieval algorithm

The robust SST is based on work done by Barton et al, 1989, for the Along Tracking Scanning Radiometer (ATSR). The method uses 1 channel in the MWIR around 3.7 μm and 2 channels in the LWIR around 10.8 and 12.0 μm, which are affected differently by the water vapor continuum. To study the improvement for 5 channels we selected 2 in the MWIR and 3 in the LWIR. A spectral channel combination was chosen which does not make use of the water vapor continuum in the 10 to 12 μm region. We found that locating two of the 5 channels near water absorption wavelengths gave similar performance to a system which had used the split channel technique (Topliss, 1995). Additionally, we found that the RMSE SST error was cut in half by combining radiances from two looks taken within a few minutes from each other: one at nadir and one at 60 degrees from nadir. During the daytime channel 1 is contaminated with scattered solar radiation and thus must be eliminated in the SST

Band Name	1	2	3	4	5
λ_{lower}	3.5	4.85	8.0	8.4	10.15
λ_{upper}	4.1	5.05	8.4	8.85	11.4
Emissivity (nadir)	.975	.975	.985	.985	.985
Emissivity (60^o)	.935	.935	.950	.950	.950

Table 2. Band limits for a 5 channel sensor and water emissivities (from Barton et al, 1989) used in this study.

$truePI \backslash chosenPI$	dry	medium	wet
dry	0.26	0.38	0.52
medium	0.43	0.38	0.60
wet	0.83	0.68	0.50

Table 3. RMSE Temperature retrieval error in K using right and wrong atmospheric prior information (PI) and 8 measurements

estimation. The basic equation for the robust SST algorithm for SST estimate $\hat{T}$ can then be written in terms of TOA brightness temperatures $T_{w,i}$ as:

$$\hat{T_w} = T_0 + \sum_{i=1 \ or \ 2}^{5} a_i T_{w,i}(nadir) + b_i T_{w,i}(60deg), \tag{3}$$

where the weighting coefficients T_0, a_i and b_i are determined using a linear procedure. $T_{w,i}$ are the TOA brightness temperatures obtained using eq.(2). Details of the algorithm have been published elsewhere (Tornow et al, 1994). We repeat the channel band limits and used water emissivities here for completeness and further reference in Table 2. Note that this algorithm assumes that the atmosphere is stratified the same for both looks, a condition violated in the presence of water vapor inhomogeneities and/or cirrus clouds.

3.1. Results:

In order to match the wide range of possible conditions we divided the atmospheric conditions into three regions: dry ($0.09 - 2.05\ g/cm^2$), medium (1.84 - 3.27 g/cm^2) and wet (3.07 - 4.19 g/cm^2). For each region a set of 9 weighting coefficients for eq.(3) were computed (5 nadir looks and 3 off-nadir looks). All atmospheric states include no or high/low altitude sub-visual cirrus with up to 0.5km geometrical thicknesses the SST was between 273 and 290 K.

From an unpublished report by Tornow and Borel from 1994 we repeat one salient result of the performance of the robust SST retrieval method. Table 3 illustrates the importance of using the correct prior information. There is an increase of the RMSE temperature error when the wrong prior information (which set of weighting coefficients) was selected.

Effects of degraded spatial resolutions for the off-nadir looks were not taken into account. For large weighting coefficients for off-nadir look temperature images the SST image could potentially be degraded to the spatial resolution of the off-nadir data.

4. Physics-based SST retrieval algorithm

In the previous section we have seen that the robust algorithm uses a linear fit to measured top-of-the-atmosphere (TOA) brightness temperatures for nadir and off-nadir (60 degrees) looks. Unfortunately the algorithm relies on a large set of atmospheric cases which is complex to compute. However, once the weighting coefficients in eq.(3) are determined the method is very simple and fast to use.

A physics-based algorithm was developed to check the consistency of the robust SST retrievals. The main idea is that the atmospherically-corrected SST temperature should be the same in all thermal channels. The measured radiance for channel i can be modeled as:

$$L_{m,i} = \varepsilon_{w,i} B_i(T_w) \tau_i(CW) + B_i(T_a)[1 - \tau_i(CW)] \tag{4}$$

Channel i	A_i	B_i	C_i
1	0.075340	0.069172	0.855049
2	0.041819	0.778816	0.666231
3	0.121604	0.304723	0.768838
4	0.047997	0.158434	0.836417
5	0.022321	0.073105	1.390880

Table 4. Coefficients to fit the transmission in 5 channels for variable water vapor amounts for a US Standard Atmosphere.

where ε_w is the water emissivity, $B_i(T)$ is the band-averaged Planck function for band i, with the subscripts w indicating water and a indicating the atmosphere. Note we neglect the reflected down-welling radiance of the atmosphere because it is a small contribution over high-emissivity water surfaces. The columnar water vapor dependent transmission is written as $\tau_i(CW)$. Solving eq.(4) for the estimated SST temperature $\hat{T}_{w,i}$ for the i-th channel:

$$\hat{T}_{w,i}(CW, T_a) = B^{-1}[\frac{L_{m,i} - B_i(\hat{T}_a)(1 - \tau_i(\hat{CW}))}{\varepsilon_{w,i}\tau_i(\hat{CW})} - \delta T_i] \tag{5}$$

where $B^{-1}[]$ indicates the inverse band-averaged Planck function.

The known quantities are the measured radiance at the sensor $L_{m,i}$ and the surface emissivity $\varepsilon_{w,i}$; the unknown quantities are the effective atmospheric temperature T_a and the columnar water vapor CW. We introduce an offset temperature $\delta T_{w,i}$ here to compensate for errors introduced by the calculation of the band-averaged quantities using different versions of MODTRAN that have different ways to change the columnar water and that have different spectral resolutions (since MODTRAN was relatively new at the time these calculations were performed in 1994 the older LOWTRAN mode was actually used which reports data every 10 cm^{-1}). While the introduction of such a temperature offset is not very elegant, it might be a useful tuning mechanism for an operational system.

Using a network of radiometers, such as the one planned to be deployed at Lake Tahoe for the vicarious calibration of MODIS and ASTER, we will be able to generate δT_i from coincident observations for a number of different atmospheres. For now however these offset temperatures can be calculated using the algorithm steps described below. For example if we need $\delta T_{w,i}$ for a desired average water temperature, e.g. T_w=300 K, for each standard atmosphere using a 23 km visibility by computing the retrieved SST for the smallest RMSE temperature we simply :

$$\delta T_{w,i} \;=\; \hat{T}_{w,i} - T_w, \text{ where } RMSE(\hat{T}_{w,i}, T_w) = minimum, \tag{6}$$

where we set $\delta T_{w,i} = 0$ in eq.(5). Using this method we force the retrieved temperature error to zero for a water surface at 300 K. For the US standard atmosphere we obtained $\delta T_{w,i} = [-0.657, 1.122, -0.962, -0.205, 0.702]$.

J. Johnson and W. Clodius found (internal communication, 1995) that the following equation is a very good approximation for the band-averaged atmospheric transmission $\tau_i(CW)$:

$$\tau_i(CW) = \exp[-(\frac{A_i}{\cos\theta} + B_i(\frac{CW}{\cos\theta})^{C_i})] \tag{7}$$

where A_i, B_i and C_i are fitting parameters obtained by varying the columnar water vapor for nadir looks. In Table 4 we list the fitting coefficients for one of the four standard atmospheres we used. The fitting coefficients were obtained by scaling the water vapor amount in each atmospheric layer and running MODTRAN 2 for these new custom profiles. Note that the relation between optical depth and columnar water amount is very nonlinear for channels K and L, which have many water absorption lines.

4.1. Algorithm steps:

1. Find pixels with water in the image.

2. For standard atmospheres (e.g. k=mid-latitude winter, US standard, mid-latitude summer and tropical):

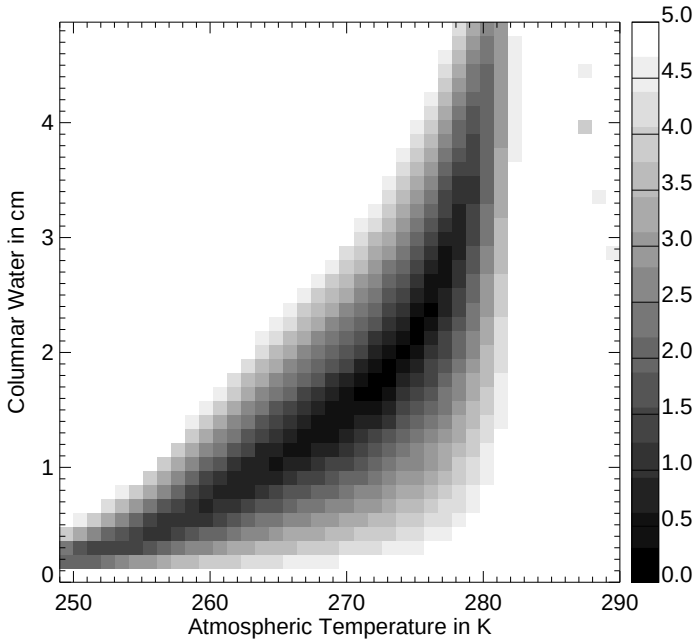

Figure 4. Standard deviation of the retrieved SST as a function of columnar water vapor and effective atmospheric temperature for $\sigma(\hat{T}_{w,i}) < 5$ K for a SST of 300 K and clear US standard atmosphere with 1.6 g/cm^2 water vapor.

(a) Change the columnar water vapor and atmospheric temperature over a range of expected values until the retrieved surface temperatures $\hat{T}_{w,i}$ are most similar, i.e. minimize the standard deviation (STDEV) for all spectral channels i or mathematically: $\sigma_k = STDEV(\hat{T}_{w,i}) = minimum$.

(b) Use the columnar water amount CW_{opt} and effective atmospheric temperature $T_{a,opt}$ in eq.(5) to retrieve the temperatures for all other water pixels.

3. Select the standard atmosphere k which is the best fit based on the smallest standard deviation σ_k of retrieved water temperatures $\hat{T}_{w,i}$.

4.2. Results for single-pixel SST retrieval:

The results of the physics-based algorithm were obtained by computing a TOA radiance set of 5 band-integrated radiances for 5 different surface temperatures using one of the 480 atmospheric cases discussed in the section on the robust SST retrieval. In Table 5 we list the true SST T_w, the standard deviation $\sigma(\hat{T}_{w,i})$ over the estimated SST's and the temperature error $\hat{T}_w - T_w$, where $\hat{T}_w$ is the average over $\hat{T}_{w,i}$. Equation (5) was used with the transmission model of equation (4) to estimate the SST in each channel.

The SST's in each channel were computed on a grid of equally spaced atmospheric temperatures over a range from 250 to 289 K in 1 K steps and for columnar water vapor amounts ranging from 0 to 4.875 g/cm^2 in steps of 0.125 g/cm^2. We did not attempt to use an optimization method to find the optimum solution. In Fig 4 the standard deviation of the retrieved SST is shown as a function of CW and T_a. Note, there are some isolated points on the right side of the plot which come about from the way the standard deviation is calculated. As the atmospheric parameters are changed it may happen that some atmospherically corrected radiances become negative as the atmospheric temperature increases. We just eliminated such radiances in the inverse Planck function computation and calculated the standard deviation for the remaining invertible positive radiances.

In Table 5 we specified a clear atmosphere (case A) for the left table and a 0.2 km thick low cirrus cloud for the right table (case B), both have a US standard atmosphere and rural aerosol (23 km visibility) with 1.6 g/cm^2

A: Clear US Standard Atmosphere			
Atmosphere	T_w	$\sigma(\hat{T}_{w,i})$	$\hat{T}_w - T_w$
Winter	280	0.173	0.223
Standard	280	0.134	0.304
Summer	280	0.141	0.348
Tropic	280	0.174	0.179
Winter	290	0.257	-0.272
Standard	290	0.159	-0.253
Summer	290	0.126	-0.300
Tropic	290	0.111	-0.261
Winter	300	0.250	-0.118
Standard	300	0.000	-0.175
Summer	300	0.208	0.014
Tropic	300	0.245	-0.269
Winter	310	0.307	-0.375
Standard	310	0.145	-0.084
Summer	310	0.392	-0.319
Tropic	310	0.499	-0.496
Winter	320	0.391	-0.088
Standard	320	0.239	-0.024
Summer	320	0.541	-0.196
Tropic	320	0.661	-0.248

B: 0.2 km thick low cirrus US Std. Atm.			
Atmosphere	T_w	$\sigma(\hat{T}_{w,i})$	$\hat{T}_w - T_w$
Winter	280	0.195	0.120
Standard	280	0.155	0.163
Summer	280	0.158	0.206
Tropic	280	0.197	0.031
Winter	290	0.291	-0.460
Standard	290	0.195	-0.447
Summer	290	0.136	-0.207
Tropic	290	0.129	-0.264
Winter	300	0.281	-0.342
Standard	300	0.057	-0.405
Summer	300	0.164	-0.224
Tropic	300	0.238	-0.505
Winter	310	0.346	-0.049
Standard	310	0.113	-0.341
Summer	310	0.373	-0.437
Tropic	310	0.492	-0.003
Winter	320	0.423	-0.193
Standard	320	0.194	-0.306
Summer	320	0.495	-0.188
Tropic	320	0.626	-0.253

Table 5. SST temperature retrieval results for a clear (atmospheric case A, left) and .2km thick low cirrus (atmospheric case B, right) US standard atmosphere with 1.6 cm^{-2} water vapor and rural aerosols (23 km visibility) for 5 temperatures.

columnar water vapor amount. For the clear atmosphere the estimated columnar water vapor amount ranged from 0.5 to 2.5 g/cm^2 while the effective atmospheric temperature $\hat{T}_a$ varied from 268 to 279 K. This behavior is expected from Fig. 4 which shows a band of possible solutions minimizing $\sigma(\hat{T}_{w,i}$. For the low cirrus case the estimated columnar water vapor amounts ranged from 0.625 to 2.375 g/cm^2 and the effective atmospheric temperature $\hat{T}_a$ ranged from 269 to 280 K.

We repeated the calculations described above for just 4 channels and found the temperature error was higher than 1 K for higher SST's and moist atmospheres, but still less than 0.5 K for all other cases. Thus we believe we will be able to use this method for day and night time data sets.

Now we investigate the effect of having a much more complex atmospheric case. Using a tropic atmosphere with high cirrus of 0.2 km thickness , urban aerosols and a water vapor amount of 3.1 g/cm^2 (atmospheric case C), we found excellent agreement of less than 0.5 K near the nominal 300 K SST that was used to compute the δT_i offset temperatures. The error increased to 1.1 K for a SST of 290 K and to 1.5 K for 310 K. Larger errors of 4.6 and -2.5 K were computed for SST's of 280 and 320 K. The retrieved CW was 0.125 - 3.375 g/cm^2 and the effective atmospheric temperature was 272-280 K. The small standard deviation $\sigma(\hat{T}_{w,i})$ clearly indicated that a tropical atmosphere was used.

One observation is that there seems to be no easy way to retrieve CW and T_a consistently for a range of SST. With 4 to 5 channels the temperature retrieval accuracy is better than 0.5 K for a range of SST's and is insensitive to the retrieved CW and T_a. A possible solution to this problem lies in using other spectral channels, e.g. near the 940 nm water vapor absorption feature, to estimate the water vapor independently. Unfortunately this is difficult over water since the water's reflectivity is very low in the near infrared. Using the atmospheric pre-corrected differential absorption (APDA) technique (Schlaepfer et al, 1998) it is possible to estimate CW over water given high sensor SNR and hazy conditions. Given such an estimate of CW it should then be possible to get a better estimate of T_a. If we however are only interested in a good estimate of SST we can use the single-pixel

A: Clear US Standard Atmosphere			
Atmosphere	$RMSE(\hat{T}_{w,i}, T_w)$	CW_{opt}	$T_{a,opt}$
Winter	0.760	2.25	274
Standard	0.185	2.00	274
Summer	0.377	1.75	274
Tropic	0.377	1.75	274

B: 0.2 km thick low cirrus US Standard Atmosphere			
Atmosphere	$RMSE(\hat{T}_{w,i}, T_w)$	CW_{opt}	$T_{a,opt}$
Winter	1.783	2.25	274
Standard	0.581	2.00	274
Summer	0.612	1.75	274
Tropic	0.612	1.75	274

Table 6. RMSE Temperature error using multi-SST retrieval for two atmospheres.

method with the understanding that the retrieved effective atmospheric temperature and columnar water vapor amount could be totally wrong.

4.3. Multi-pixel SST retrieval:

The results in the previous sub-section suffer from the inability to retrieve consistent CW and T_a. However for a special case it is possible to retrieve both atmospheric parameters with quite acceptable accuracy. Running the previous methods we discovered a similarity of the standard deviation $\sigma(\hat{T}_{w,i})$ of the retrieved brightness temperatures as a function of CW and T_a for different SST's (see Figure 4). All show an upward sweeping valley of good solutions which minimize $\sigma(\hat{T}_{w,i})$. In Figure 5 we plot the location of the local minima for a fixed atmospheric temperature using symbols for the 5 different SST's. We can see clearly that the minima seem to converge at a particular C and T_a location that could be determined by computing intersections of curve fits to the plotted points. However, a much more elegant method was suggested which has been used to verify that the optimum CW and T_a location can be used to accurately retrieve SST's. The following additional steps need to be implemented:

1. Select a number of temperatures over a range of SST's of interest, e.g. we just used the previously discussed 5 temperatures $T_{w,j} = 280,\ 290,\ 300,\ 310,\ 320$ K.
2. Compute $\sigma(\hat{T}_{w,i})$ as a function of CW and T_a for each temperature $T_{w,j}$.
3. Compute the average of all standard deviations over N_{temp} temperatures:

$$\sigma_{avg}(CW, T_a) = \frac{1}{N_{temp}} \sum_{j=1}^{N_{temp}} \sigma(\hat{T}_{w,j})$$

4. Find the optimum CW and T_a by finding the minimum of $\sigma_{avg}(CW, T_a)$. In Figure 6 we plot the region where $\sigma_{avg}(CW, T_a) < 1$ K.
5. Run the physics-based SST using the found optimal values of CW and T_a.

The retrieved atmospheric parameters and the SST RMSE are listed in Table 6 for each atmosphere type. Note the small SST RMSE of 0.185 K for the standard atmosphere case for the large range of covered SST's. The RMSE is 0.58 K for atmospheric case B. Both retrievals show the atmospheric temperature at 274 K for all atmospheres and the retrieved water vapor amount is not far from the 1.6 g/cm^2 reported by MODTRAN.

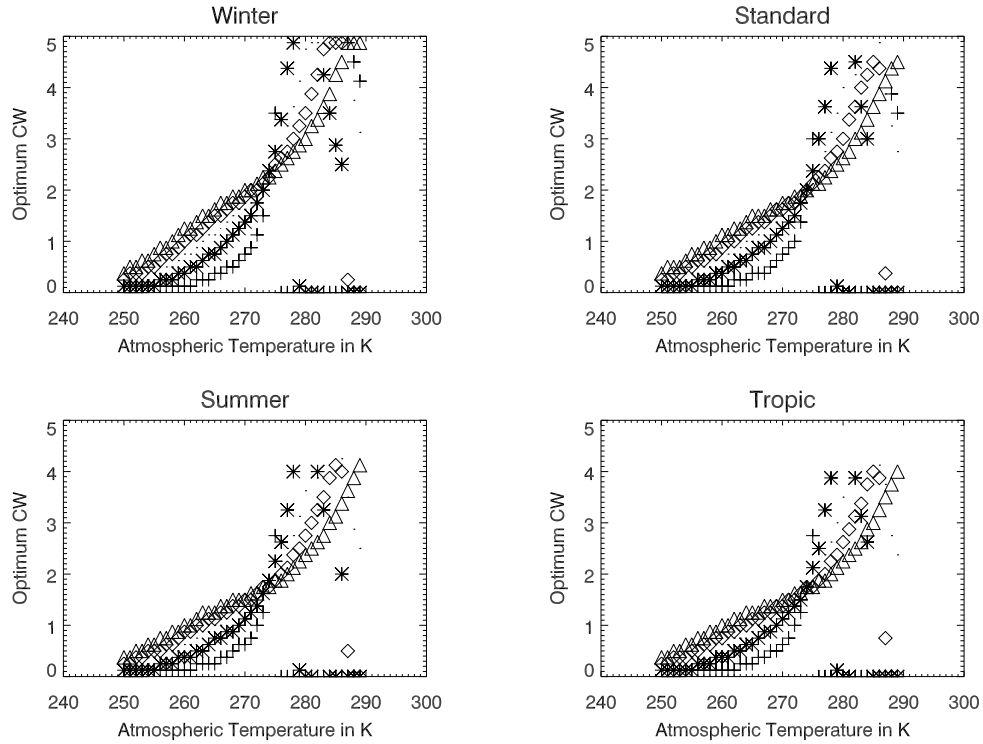

Figure 5. Local minima of $\sigma(\hat{T}_{w,i})$ for fixed T_a along the CW axis for atmospheric case B.

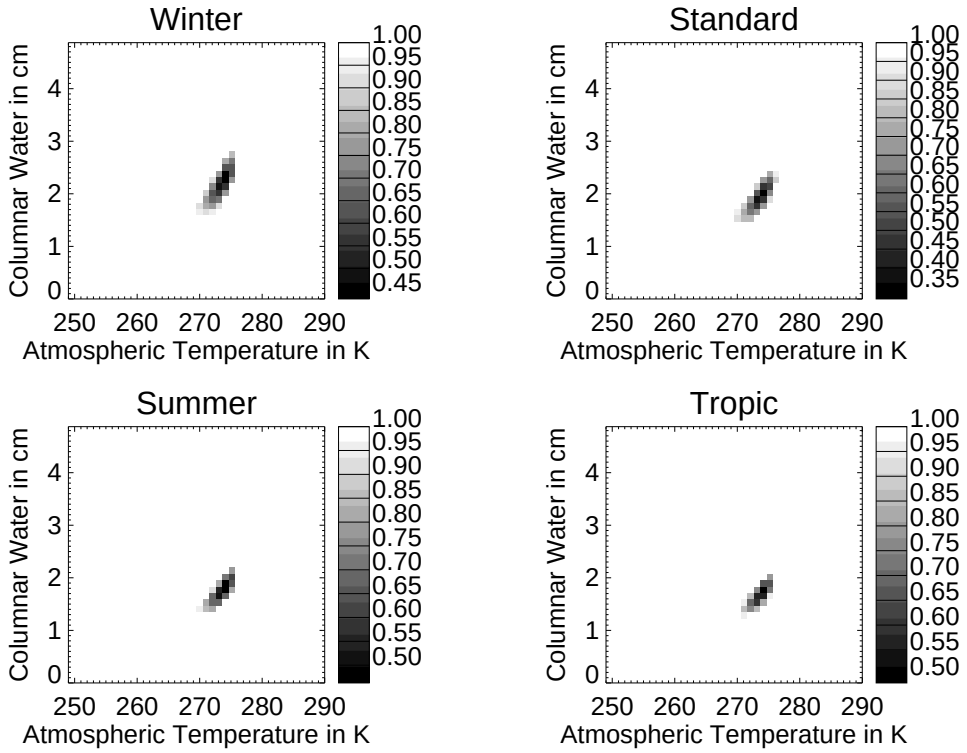

Figure 6. Average standard deviation $\sigma_{avg}(CW, T_a)$ for 5 SST's for atmospheric case B.

5. Discussion

The two described SST retrieval methods have similar errors in temperature retrievals.

The robust method is insensitive to many atmospheric conditions and should be used when little information is available over a site of interest. The two-looks required by the method to achieve a good SST retrieval are challenging to realize and may lead to a spatial degradation of the SST map.

The physics-based method yields better results when the approximate atmospheric state is known and most importantly does not require a second look to improve the accuracy. The physics-based method retrieves in general very accurate SST but fails to retrieve usable CW and T_a for single-pixel SST retrievals. When multiple temperatures are present in a scene with a homogeneous atmosphere the physics-based multi-pixel SST retrieval is able retrieve meaningful CW and T_a values.

If the columnar water can be determined by other means (e.g. APDA, using sun-glint views over water) then the SST can be determined on a pixel-by-pixel basis for an in-homogeneous atmosphere. We hope to extend the physics-based method to retrieve emissivities and temperatures over land which may be possible if water bodies are present and for data which includes water vapor information.

6. Acknowledgements

The authors acknowledge the very important contributions by former postdoctoral associate Dr. Carmen Tornow (now with the German Aerospace Research Establishment (DLR) in Berlin, Germany) who laid the groundwork for the robust SST used in this paper. Tony Crider and Jennifer Johnson also provided us with valuable contributions over the years to run MODTRAN over many iterations and harness its data. Dr. Barry Smith had the idea of adding up the standard deviations in sub-section 4.3. We also acknowledge the leadership and encouragement of Dr. Paul Weber and the financial support from the Department of Energy under contract W-7405-ENG-36. Part of this work was also supported by a grant from NASA HQ to study temperature retrievals in complex environments (NASA W-19,324).

References

Barton, I.J., A.M. Zavody, D.M. O'Brien, D.R. Cutten, R.W. Saunders and D.T. Llewellyn-Jones, "Theoretical algorithms for satellite-derived sea surface temperature," J.Geophys. Res., 94:D3, pp.3365-3375, 1989.

C.C. Borel, B.J. Cooke and B.E. Laubscher, "Partial removal of correlated noise in thermal imagery," SPIE AeroSense'96, Proc. Vol. 2759, pp.131-138, April 1996.

D. Schlaepfer, C.C. Borel, J. Keller and K.I. Itten, "Atmospheric pre-corrected differential absorption technique to retrieve columnar water vapor", RSE Vol. 65, no. 3, pp353-366, 1998.

Sobrino, J.A., Li, Z.H., and Stoll, M.P., "Impact of the atmospheric transmittance and total water vapor content in the algorithms for estimating satellite sea surface temperatures," IEEE Transactions on Geoscience and Remote Sensing, 31, 1993.

Szymanski, J.J., C.C. Borel, Q.O. Harberger, P.Smolarkiewicz and J. Theiler, "Subpixel temperature retrieval with mulispectral sensors," Aerosense'99, SPIE conference proceedings, Vol. 3717.

Topliss, B.J., "A review of satellite sea surface temperature validations for NOAA'S 7,9, and 11 using imagery off eastern Canada," Canada J. of Remote Sensing, 21, 1995.

Tornow, C., C.C. Borel, and B.J. Powers, "Robust water temperature retrieval using multi-spectral and multi-angular IR measurements," Proc. IGARRS '94, 441-443, 1994.